JOURNAL OF GEOPHYSICAL RESEARCH, VOL. 114, A07103, doi:10.1029/2008JA013990, 2009

Asymmetric shear flow effects on magnetic field configuration within oppositely directed solar wind reconnection exhausts

S. Eriksson,[1] J. T. Gosling,[1] T. D. Phan,[2] L. M. Blush,[3] K. D. C. Simunac,[4] D. Krauss-Varban,[2] A. Szabo,[5] J. G. Luhmann,[2] C. T. Russell,[6] A. B. Galvin,[4] and M. H. Acuña[7,8]

Received 12 December 2008; revised 27 February 2009; accepted 4 May 2009; published 18 July 2009.

[1] We present observations of the nearly oppositely directed solar wind reconnection jets from the same reconnection X line that swept by the Wind and STEREO-A spacecraft on 11 March 2007. The event was characterized by an external plasma density asymmetry and a jet-aligned shear flow across the exhausts. A well-defined pair of asymmetric current sheets bounded both outflow regions. The observed current sheet asymmetries and differences in the magnitude of the antiparallel magnetic field components within the two exhausts were consistent with the sense of the shear flow and the predictions from two-dimensional MHD simulations of reconnection outflows for the Earth's asymmetric flank magnetopause.

Citation: Eriksson, S., et al. (2009), Asymmetric shear flow effects on magnetic field configuration within oppositely directed solar wind reconnection exhausts, *J. Geophys. Res.*, *114*, A07103, doi:10.1029/2008JA013990.

1. Introduction

[2] Magnetic reconnection is a universal plasma process that changes the magnetic field configuration and allows for a mixing of plasmas from disparate regions initially separated by a tangential field discontinuity [*Priest and Forbes*, 2000]. Asymmetric reconnection commonly occurs at the Earth's magnetopause [e.g., *Levy et al.*, 1964; *Paschmann et al.*, 1979; *Sonnerup et al.*, 1981; *Lin and Lee*, 1994] which separates plasmas of different plasma density, temperature, and field strengths.

[3] The telltale signature of magnetic reconnection in the solar wind consists of a pair of oppositely directed plasma jets. A single spacecraft typically samples only one of the exhausts. The roughly Alfvénic-accelerated outflow plasma jet is bounded by correlated changes in magnetic field (**B**) and velocity (**V**) on one side and anticorrelated changes in **B** and **V** on the other side of the exhaust.

[4] Reconnection exhausts have been observed over a wide range of heliocentric distances (0.3–5.4 AU) and are often associated with extended (hundreds of Earth radii) reconnection X lines [e.g., *Gosling et al.*, 2005, 2006a, 2006b, 2007a; *Phan et al.*, 2006]. Solar wind reconnection often occurs in current sheets that separate plasmas of asymmetric density and magnetic field strength [e.g., *Gosling et al.*, 2005]. The relatively constant motion of these current sheets past spacecraft provides ideal conditions for the analysis of their structure.

[5] This report compares in situ observations from STEREO-A (ST-A) and Wind on opposite sides of an extended X line in the low-speed solar wind on 11 March 2007 with MHD predictions of asymmetric reconnection exhausts. The large spatial extent and duration of this event was discussed in considerable detail by *Gosling et al.* [2007b]. In extending this study, we demonstrate that an external jet-aligned shear flow is an important factor in determining the asymmetric nature of the pair of current sheets that bound the outflow and thus the outflow magnetic field configuration. This has been predicted on the basis of 2-D MHD simulations of asymmetric reconnection exhausts at the Earth's flank magnetopause [*La Belle-Hamer et al.*, 1995]. Our report provides the first direct comparison of these asymmetric reconnection predictions with solar wind observations.

2. Wind and STEREO Observations of Opposite Exhausts

[6] A current sheet with reconnection signatures was observed in the solar wind on 11 March 2007 by ST-A (0338–0343 UT), ACE (0526–0528 UT), Wind (0545–

[1]Laboratory for Atmospheric and Space Physics, University of Colorado at Boulder, Boulder, Colorado, USA.
[2]Space Sciences Laboratory, University of California, Berkeley, California, USA.
[3]Physikalisches Institut, University of Bern, Bern, Switzerland.
[4]Space Science Center, University of New Hampshire, Durham, New Hampshire, USA.
[5]Heliospheric Physics Laboratory, NASA Goddard Space Flight Center, Greenbelt, Maryland, USA.
[6]Institute of Geophysics and Planetary Physics, University of California, Los Angeles, California, USA.
[7]Solar System Exploration Division, NASA Goddard Space Flight Center, Greenbelt, Maryland, USA.
[8]Deceased 5 March 2009.

0148-0227/09/2008JA013990$09.00

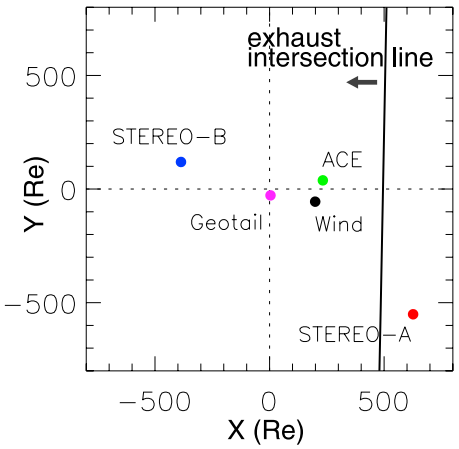

Figure 1. Five spacecraft GSE positions at the time of individual exhaust encounters on 11 March 2007. The Z_{GSE} positions (R_E) of all five spacecraft were −33.7 (ST-A), −16.8 (Wind), −14.6 (ACE), −6.8 (Geotail), and −25.3 (ST-B). The intersection of the XY_{GSE} plane (0, 0, 1) with the exhaust cross-product normal at ST-A (see Table 1) is also shown. The exhaust is carried antisunward by the solar wind flow (arrow).

0549 UT), Geotail (0641–0647 UT), and STEREO-B (ST-B) (0858–0901 UT). Figure 1 shows the individual locations of all five spacecraft in Earth radii (1 R_E = 6378 km) and GSE coordinates when they encountered the exhaust intersection with the ecliptic plane (tilted solid line). The five spacecraft were located between Z_{GSE} = −6.8 R_E (Geotail) and Z_{GSE} = −33.7 R_E (ST-A). All spacecraft except for ST-A observed a sunward directed plasma jet.

[7] Figure 2 presents a 30-min interval of Wind and ST-A magnetic field [*Lepping et al.*, 1995; *Acuña et al.*, 2008] and plasma data [*Lin et al.*, 1995; *Galvin et al.*, 2008] centered at the Wind exhaust region (shaded). The high-resolution proton density (N_p) measured by the Wind Three-Dimensional Plasma investigation (3DP) instrument [*Lin et al.*, 1995] was scaled according to N_p/0.573 to match the 0000–1200 UT average N_p from the Wind Solar Wind Experiment (SWE) instrument [*Ogilvie et al.*, 1995]. The scaling was required by the offset of the onboard 3DP density calibration at this time. The top three panels of Figure 2 demonstrate that the spacecraft observed oppositely directed outflows (accelerated solar wind speed at ST-A, decelerated speed at Wind) and that both spacecraft moved from a high-density to a low-density region.

[8] The magnetic field and velocity in Figure 2 are shown in orthogonal (L, M, N) boundary normal components, where $\hat{\mathbf{L}}$ is a unit vector aligned with the outflow direction, $\hat{\mathbf{N}}$ is a unit normal of the equilibrium current sheet prior to reconnection, and $\hat{\mathbf{M}} = \hat{\mathbf{N}} \times \hat{\mathbf{L}}$ which is assumed to be parallel to the X line. These $\hat{\mathbf{L}}$, $\hat{\mathbf{M}}$, and $\hat{\mathbf{N}}$ directions were individually obtained at ST-A and Wind as follows. We first assume that $\hat{\mathbf{N}} = (\mathbf{B}_1 \times \mathbf{B}_2)/|\mathbf{B}_1 \times \mathbf{B}_2|$, where $\mathbf{B}_1$ and $\mathbf{B}_2$ are average magnetic field directions before and after the reconnection exhausts, respectively. We then employ a minimum variance analysis (MVAB) technique [*Sonnerup and Scheible*, 1998] on the 1-s ST-A and the 3-s resolution Wind **B** GSE data across the exhausts to find a maximum variance direction $\hat{\mathbf{L}}_0$. An $\hat{\mathbf{L}}$ direction orthogonal to $\hat{\mathbf{N}}$ is derived as $\hat{\mathbf{L}} = \mathbf{L}_\perp/|\mathbf{L}_\perp|$, where $\mathbf{L}_\perp = \hat{\mathbf{L}}_0 - \mathbf{L}_\parallel$ and $\mathbf{L}_\parallel = (\hat{\mathbf{L}}_0 \cdot \hat{\mathbf{N}})\,\hat{\mathbf{N}}$. The final ST-A and Wind $\hat{\mathbf{N}}$, $\hat{\mathbf{L}}$, and $\hat{\mathbf{M}}$ (GSE) that we use in Figure 2 to transform the measured magnetic field and velocity (GSE) are shown in Table 1 together with the average $\mathbf{B}_1$ and $\mathbf{B}_2$ vectors. We also tabulate the minimum variance MVAB normal $\hat{\mathbf{N}}_0$ in Table 1 for comparison with the cross-product normal $\hat{\mathbf{N}}$. The angles between $\hat{\mathbf{N}}$ and $-\hat{\mathbf{N}}_0$ were 7.8° (ST-A) and 5.5° (Wind), respectively. The two $\hat{\mathbf{L}}$ directions which we obtained individually at Wind and ST-A are only 24.3° apart despite the large separation between Wind and ST-A (see Figure 1). This confirms that the two jets at Wind and ST-A were

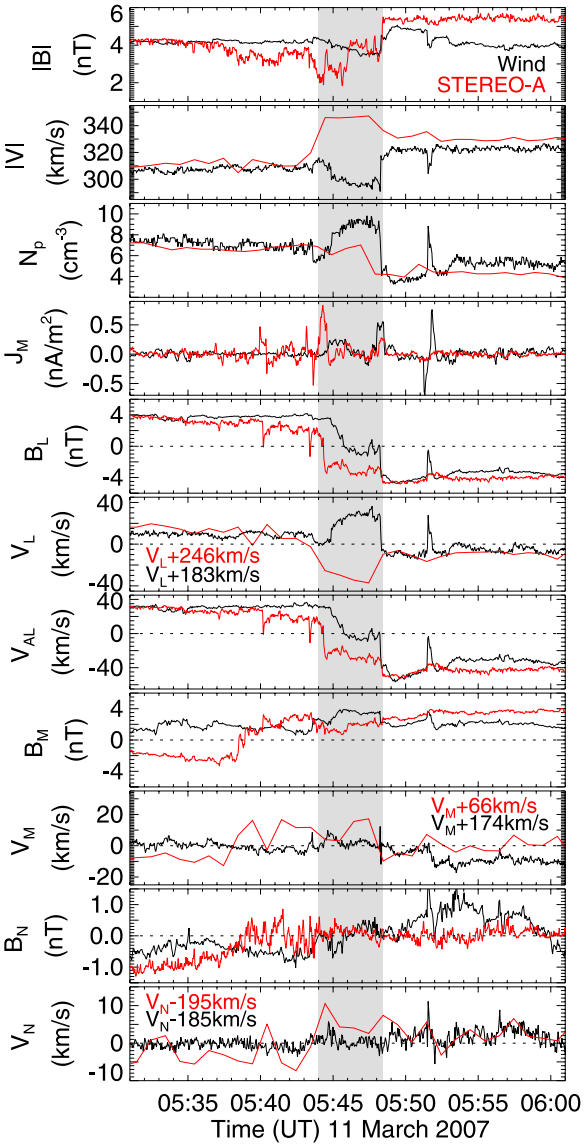

Figure 2. Plasma and magnetic field observations in LMN coordinates at Wind (black) and ST-A (red) on 11 March 2007. The ST-A data were shifted forward in time by 126 min to match up with the Wind measurements and the plasma velocity is shown in the solar wind frame of reference. The shaded region marks the exhaust regions.

Table 1. Boundary Normal Coordinate System Unit Vectors $\hat{\mathbf{N}}$, $\hat{\mathbf{L}}$, and $\hat{\mathbf{M}}$ for ST-A and Wind[a]

	ST-A	Wind
T_1 (UT)	0337:48–0338:00	0544:19–0544:28
T_2 (UT)	0342:45–0342:57	0548:22–0548:31
$\mathbf{B}_1$ (nT)	(1.96, −1.29, −1.39)	(3.48, 0.54, −2.34)
$\mathbf{B}_2$ (nT)	(−3.06, −3.96, 2.10)	(−0.83, −4.16, 1.17)
$\hat{\mathbf{N}}$[b]	(−0.5741, 0.0110, −0.8187)	(−0.5395, −0.1274, −0.8323)
$\hat{\mathbf{L}}$	(0.7863, 0.2862, −0.5475)	(0.5874, 0.6513, −0.4805)
$\hat{\mathbf{M}}$	(0.2283, −0.9581, −0.1730)	(0.6033, −0.7481, −0.2765)
$\hat{\mathbf{N}}_0$[b]	(0.5253, 0.1126, 0.8434)	(0.5441, 0.0315, 0.8384)
$\hat{\mathbf{L}}_0$	(0.7958, 0.2860, −0.5338)	(0.6201, 0.6580, −0.4272)
$\hat{\mathbf{M}}_0$	(−0.3014, 0.9516, 0.0606)	(−0.5651, 0.7524, 0.3385)

[a]$\hat{\mathbf{L}}_0$, $\hat{\mathbf{M}}_0$ and $\hat{\mathbf{N}}_0$ correspond to MVAB maximum, intermediate, and minimum variance eigenvectors. All vectors are shown in GSE coordinate system.
[b]Note that the normals may be $\pm\,\hat{\mathbf{N}}$ and $\pm\,\hat{\mathbf{N}}_0$.

roughly oppositely directed. We also note that the average field shear angles between $\mathbf{B}_1$ and $\mathbf{B}_2$ (see Table 1) were $\omega = 105°$ across the exhaust at ST-A and $\omega = 115°$ at Wind.

[9] The MVAB technique was applied on the 0544–0549 UT Wind magnetic field data and resulted in eigenvalues $[\lambda_3, \lambda_2, \lambda_1] = [0.0512, 0.4079, 5.4183]$ where λ_3 is the eigenvalue for the minimum variance direction. The corresponding times and eigenvalues for the ST-A data were 0337–0344 UT and $[\lambda_3, \lambda_2, \lambda_1] = [0.0352, 0.4551, 4.7043]$. The eigenvalues are well separated and indicate high-quality $\hat{\mathbf{L}}_0$ and $\hat{\mathbf{N}}_0$ MVAB directions. However, we refrain from using the MVAB normals on the basis of the general stability of cross-product normals over all field shear angles [*Knetter et al.*, 2004] and since the ST-A cross-product normal resulted in a better overall timing of the exhausts at all five spacecraft than if we used the ST-A MVAB normal. The predicted timings of the exhausts on the basis of $\Delta t_{ij} = \Delta\mathbf{R}_{ij} \cdot \hat{\mathbf{N}}/\mathbf{V} \cdot \hat{\mathbf{N}}$ are displayed in Table 2 for reference. Here, we used an average solar wind velocity $\mathbf{V} = (-304, -8, -24)$ km/s (GSE) on the basis of the mean 20-min average velocity prior to the exhaust encounters at all spacecraft except Geotail. Table 2 compares the predicted arrival times t_1 and t_2 using the ST-A cross-product normal ($\hat{\mathbf{N}}$) and the MVAB normal ($\hat{\mathbf{N}}_0$), respectively. We note that the spacecraft timings reported by *Gosling et al.* [2007b] for this event, which predicted shorter delay times than were observed, were obtained using an incorrect ST-A MVAB normal.

[10] We recently investigated the applicability of the MVAB normals for seven narrow solar wind exhausts observed by the Wind spacecraft on 19 and 20 November 2007 [*Gosling and Szabo*, 2008]. The field shear angles across these exhausts ranged from as low as $\omega = 14°$ to $\omega = 118°$. Despite a limited data set, it was clear that the cross-product normals ($\hat{\mathbf{N}}$) resulted in small average B_N within all seven exhausts, while the MVAB normals ($\hat{\mathbf{N}}_0$) resulted in large average B_N below a critical shear angle despite large intermediate-to-minimum eigenvalue ratios λ_2/λ_3. The transition occurred for shear angles $47° < \omega < 71°$ which is consistent with the $\omega > 60°$ reported by *Knetter et al.* [2004].

[11] Given the directions of the external magnetic fields, the oppositely directed exhausts, and the direction of the cross-product normals (see Table 1), we expect a generally northward ($B_Z > 0$) or $B_N < 0$ normal field within the antisunward (ST-A) exhaust and a southward GSE field ($B_Z < 0$) or $B_N > 0$ normal field within the sunward (Wind) exhaust. This situation only seemed to be satisfied toward the low-density side of both exhaust regions (see Figure 2). Signs of B_N opposite to the prediction were found toward the high-density sides of both exhaust regions. As a comparison, the $-\hat{\mathbf{N}}_0$ MVAB normals resulted in signs of B_N which were opposite to the expectation throughout both exhaust regions.

[12] Figure 2 shows the L component of the Alfvén velocity $V_{AL} = B_L/\sqrt{\mu_0\rho}$ and the M component of the current sheet density (J_M) from Ampère's law. Here, $\mu_0 J_M = (\partial B_L/\partial N - \partial B_N/\partial L)$. This can be approximated as $\mu_0 J_M = (\Delta B_L/\Delta N - \Delta B_N/\Delta L) = (\Delta B_L/\Delta t V_N - \Delta B_N/\Delta t V_L)$, where V_N and V_L are the solar wind velocity components in the Wind and ST-A spacecraft frames of reference (see Figure 2). A clear two-step B_L decrease was observed at both spacecraft as they moved across the exhaust from $B_L > 0$ to $B_L < 0$. ST-A observed an average $B_L = -2.9$ nT within the antisunward exhaust while Wind measured $B_L = -0.6$ nT within the sunward exhaust. The ΔB_L changes at opposite exhaust boundaries correspond to a stronger out-of-plane current density $J_M = 0.83$ nA/m^2 on the high-density side as ST-A entered the exhaust while Wind detected a stronger $J_M = 0.55$ nA/m^2 as it exited into the low-density region. The weaker J_M of the bounding current sheet pair was 0.28 nA/m^2 for ST-A and 0.26 nA/m^2 for Wind. The asymmetric J_M locations on opposite sides of the respective plasma jets at ST-A and Wind coincided with the location of maximum shear flow ΔV_L between the exhaust and the adjacent region.

[13] Wind observed a narrow flow deceleration event at 0551:30 UT after the main exhaust encounter. This second feature had all the characteristics of a partial reentry into the same exhaust and suggests a local deviation of the geometry of the exhaust boundaries from infinite flat planes [*Gosling et al.*, 2007a, 2007b; *Lin et al.*, 2009]. ST-A did not observe a clear partial reentry feature after the main exhaust. However, the B_L component suggests that ST-A did observe two partial events before the exhaust transition. The bipolar J_M feature at a partial event is an analysis artifact arising

Table 2. Observed and Predicted Arrival Times for 11 March 2007 Solar Wind Exhaust

Spacecraft Pair[a]	t_{obs} (min)	t_1[b] (min)	t_2[c] (min)	$t_{obs}-t_1$ (min)	$t_{obs}-t_2$ (min)
1, 2	108.0	118.8	73.1	−10.8	34.9
1, 3	127.0	129.7	90.7	−2.7	36.3
1, 4	183.5	186.7	144.1	−3.2	39.4
1, 5	320.5	318.6	264.1	1.9	56.4
2, 3	19.0	10.9	17.6	8.1	1.4
2, 4	75.5	67.9	71.0	7.6	4.5
2, 5	212.5	199.8	191.0	12.7	21.5
3, 4	56.5	57.0	53.4	−0.5	3.1
3, 5	193.5	188.9	173.4	4.6	20.1
4, 5	137.0	131.9	120.0	5.1	17.0

[a]Spacecraft GSE positions (R_E): (1) $R_{STA} = (626.46, -550.99, -33.69)$ at 0338:00 UT; (2) $R_{ACE} = (232.47, 38.25, -14.59)$ at 0526:00 UT; (3) $R_{Wind} = (199.06, -55.47, -16.77)$ at 0545:00 UT; (4) $R_{Geotail} = (4.01, -27.82, -6.79)$ at 0641:30 UT; (5) $R_{STB} = (-386.66, 119.17, -25.34)$ at 0858:30 UT.
[b]Prediction using ST-A $\hat{\mathbf{N}} = (-0.5741, 0.0110, -0.8187)$.
[c]Prediction using ST-A $\hat{\mathbf{N}}_0 = (0.5253, 0.1126, 0.8434)$.

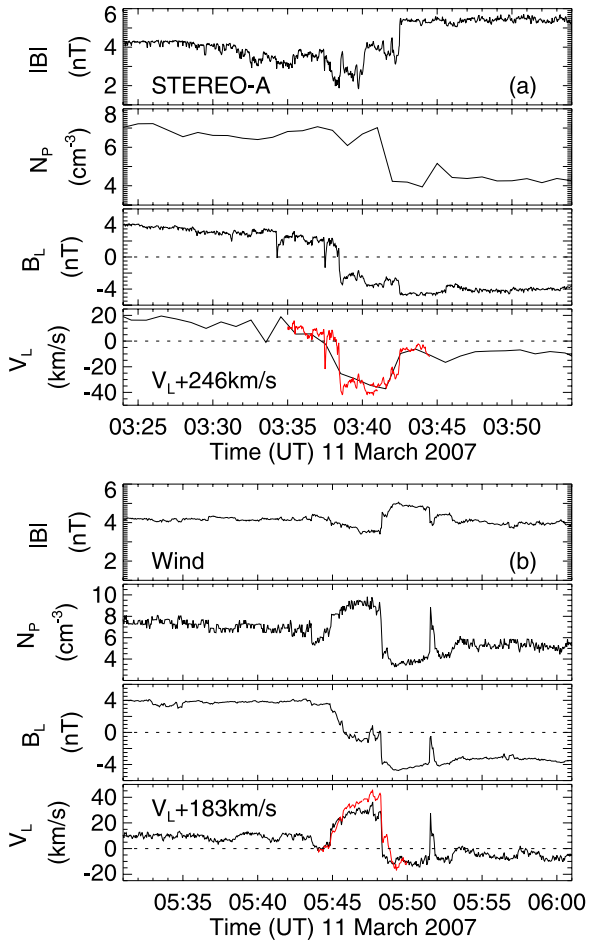

Figure 3. (a) ST-A and (b) Wind observations of total magnetic field strength, plasma density, jet-aligned B_L magnetic field component, and V_L flow in the solar wind frame of reference at the time of the respective reconnection exhausts. Red lines in the V_L panel show the predicted V_L speed from the Walén relation.

from the advancement of time in the forward direction only when applying Ampère's law.

[14] Figure 3 shows the observed total magnetic field strength, V_L in the solar wind frame, as well as the relevant N_p and B_L quantities for the Walén relation [e.g., *Sonnerup et al.*, 1981; *Paschmann et al.*, 1986]. ST-A (Wind) observations are shown in Figure 3a (Figure 3b). The red lines in the V_L panels display the predicted velocity change ΔV_L on the basis of $V_L = V_{L0} + \Delta V_L$, where V_{L0} is the reference speed adjacent to the exhaust. Here, $\Delta V_L = \sqrt{\rho_0/\mu_0}(B_L/\rho - B_{L0}/\rho_0)$, where $\rho = N_p m_p$ is the proton mass density and adjacent reference values are indicated as ρ_0 and B_{L0}. Two separate predictions were performed toward the exhaust center from either side of the exhausts using a V_{L0} before or after the event. The Walén relation was clearly satisfied across each exhaust boundary for both ST-A and Wind. This confirms that the observed magnetic field rotations were associated with an Alfvénic flow acceleration as expected for magnetic reconnection [e.g., *Paschmann et al.*, 1986]. The estimated reconnection electric fields ($E_M = -V_N B_L$) were 0.005 mV/m at Wind and 0.015 mV/m adjacent to the ST-A exhaust (see Figure 2) as compared to the 0.03 mV/m reported by *Phan et al.* [2006].

3. Simulation Predictions of Asymmetric Reconnection

[15] *La Belle-Hamer et al.* [1995] examined the effects of a jet-aligned shear flow and an asymmetric plasma density on the structure of the pair of current sheets that bound a reconnection exhaust. They used a 2-D MHD code and normalized parameters suitable for the Earth's flank magnetopause to conclude that density asymmetry and flow shear compete with one another in determining the location of the stronger boundary current sheet.

[16] Figure 4 reproduces several normalized quantities obtained by *La Belle-Hamer et al.* [1995] along normal trajectories through the oppositely directed (V_y) reconnection exhausts. Here, (x, y, z) correspond to the (−N, L, −M) components shown in Figure 2. Two asymmetric plasma density cases are compared that illustrate the expected differences for exhausts with and without a shear flow. The zero shear flow case (left) yields a stronger out-of-plane current sheet density (J_z) on the high-density side of both exhaust regions [e.g., *Karimabadi et al.*, 1999]. In the fluid picture, a larger plasma inertia and a correspondingly lower Alfvén speed require a stronger $\mathbf{J} \times \mathbf{B}$ force on the high-density side to match the exhaust outflow speed from the low-density side [*La Belle-Hamer et al.*, 1995]. A continuous change of the velocity across the exhaust is required by the frozen-in condition of the magnetic field and plasma flow outside the reconnection diffusion region. We note that identical B_y magnetic field component signatures were obtained within the opposite exhaust regions (top and bottom) in the zero shear flow case.

[17] The finite shear flow case (right) illustrates an important deviation from a zero shear flow. Here, $2V_0$ corresponds to the total change in jet-aligned V_y flow (shear) across the exhaust. V_0 was normalized by the Alfvén speed at infinity. A stronger J_z now occurs at the low-density boundary of one outflow region (top right), while J_z intensified at the high-density boundary for the opposite exhaust (bottom right). These changes are consistent with the location of the maximum shear flow ΔV_y between the exhaust and the adjacent region on different sides of the X line. A larger xy-plane $\mathbf{J} \times \mathbf{B}$ force (due to J_z) is required by the larger plasma flow velocity difference $\Delta V_y = \pm \Delta V_{ay}$ because of the additional shear where $V_{ay} = B_y/\sqrt{\mu_0 \rho}$ is the jet-aligned component of the Alfvén velocity. The exhaust B_y magnitude will therefore be different on opposite sides of the X line since the external B_y and mass density ρ are assumed fixed and $\mu_0 J_z = \partial B_y/\partial x (\partial B_x/\partial y$ is negligible).

4. Discussion and Summary

[18] The solar wind reconnection exhaust that swept by ST-A and Wind on 11 March 2007 provides a rare observation of two oppositely directed plasma jets from a common X line in the presence of an asymmetric plasma density and a jet-aligned ΔV_L shear flow. The normalized *La Belle-Hamer et al.* [1995] results of the simulated behavior of J_z, V_y, and B_y for oppositely directed reconnec-

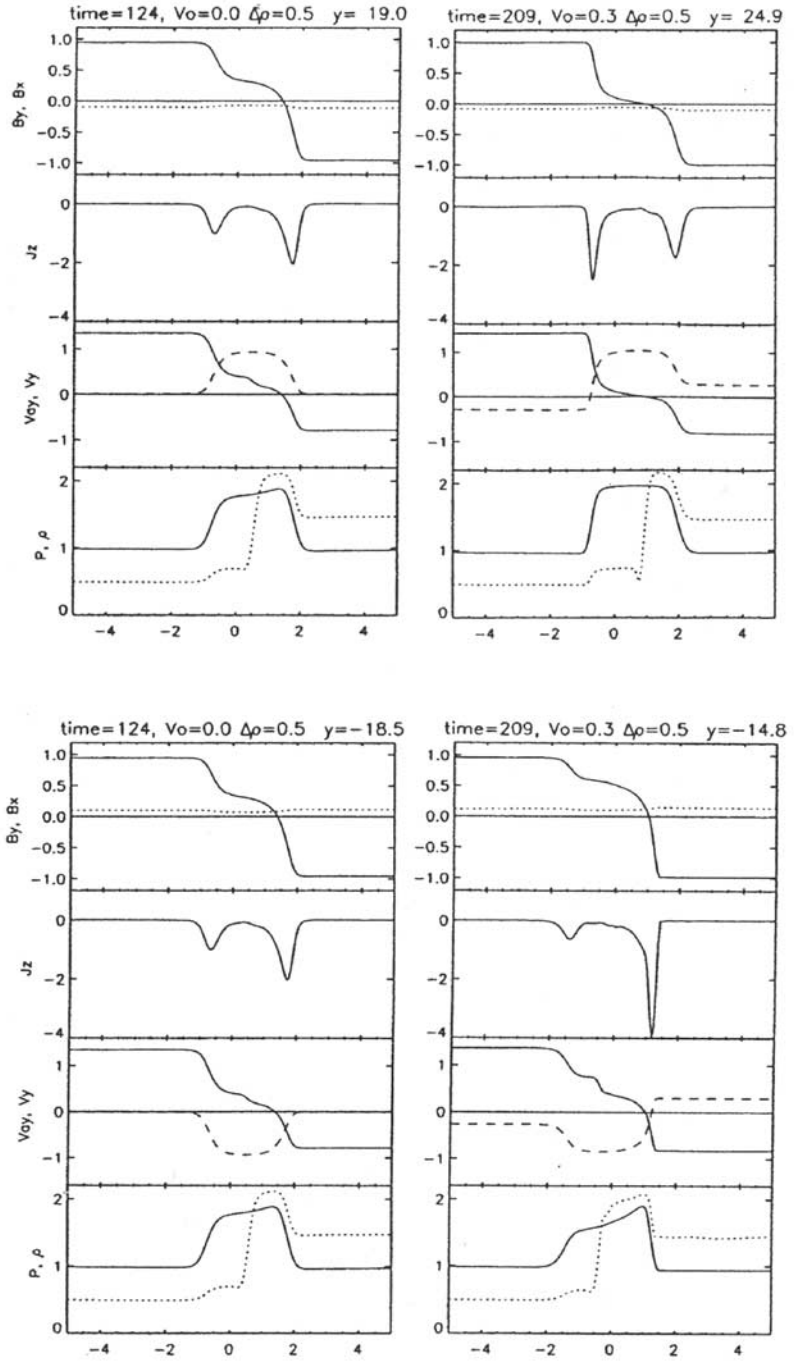

Figure 4. Horizontal slices of 2-D plane magnetic field (jet-aligned B_y, solid line; normal B_x, dashed line), current density (J_z), Alfvén and plasma velocity (V_{ay}, solid line; V_y, dashed line), pressure (P, solid line), and plasma density (ρ, dashed line) through the oppositely directed V_y jets from a 2-D MHD simulation. Values are normalized to the asymptotic magnetic field and density at infinity. A (left) zero shear flow case and a (right) finite shear flow case are compared, showing the (top) antisunward and (bottom) sunward jets. Reproduced from *La Belle-Hamer et al.* [1995].

tion exhausts (see Figure 4) in the presence of shear flow and plasma asymmetry also displayed very good agreement with the observed J_M asymmetry of the 11 March 2007 X line and the observed differences of the B_L magnetic field components within the exhausts.

[19] For a given plasma density asymmetry and assuming a satisfied Walén relation [*Sonnerup et al.*, 1981], *La Belle-Hamer et al.* [1995] predicted that the shear flow would dominate over the density asymmetry in determining the J_M structure above a threshold shear velocity $\Delta V_L^* = |V_{AL,2}| - |V_{AL,1}|$. Here, $V_{AL,i}$ is the L component of the Alfvén velocity in the adjacent low-density ($i = 2$) and high-density ($i = 1$) regions. The Walén relation was indeed satisfied across both exhaust boundaries at both ST-A and

Table 3. Average V_L and V_{AL} in the Solar Wind Frame of Reference Before and After the ST-A and Wind Exhausts

Spacecraft	High-Density Time (UT)	Low-Density Time (UT)	$V_{L,1}$ (km/s)	$V_{L,2}$ (km/s)	$V_{AL,1}$ (km/s)	$V_{AL,2}$ (km/s)	ΔV_L^T (km/s)	ΔV_L^* (km/s)
ST-A[a]	0542:00–0543:00	0548:30–0549:30	5.6	−6.2	16.8	−49.2	11.8	32.4
Wind	0544:20–0544:40	0548:25–0548:40	2.4	−6.4	30.6	−37.5	8.7	6.8
ST-A[b]	0536:00–0538:00	0555:00–0557:00	13.2	−7.2	25.1	−43.8	20.4	18.7

[a]Time intervals adjacent to ST-A exhaust. Times are in the Wind frame of reference and include the 126-min time shift.
[b]Time intervals far from ST-A exhaust.

Wind (see Figure 3) and the observed total shear flow ΔV_L^T across the Wind exhaust satisfied $\Delta V_L^T > \Delta V_L^*$ as shown in Table 3. A stronger J_M on the low-density side at Wind is therefore consistent with the MHD shear flow predictions. The $\Delta V_L^T < \Delta V_L^*$ adjacent to the ST-A jet (see Table 3) would suggest a plasma density–dominated situation. However, if observed values well upstream and downstream of the ST-A jet are used instead, one finds a shear flow–dominated situation, i.e., $\Delta V_L^T > \Delta V_L^*$. As shown in Figure 4, both cases are consistent with a stronger J_M on the high-density side.

[20] To the best of our knowledge, this is the first time that the normalized *La Belle-Hamer et al.* [1995] MHD simulation predictions of asymmetric reconnection have been successfully tested against in situ observations that require exhaust information from the oppositely directed jets and their adjacent regions. The successful comparison suggests that the same physics is involved in determining the structure of the exhaust boundary current sheets at reconnection jets in both the solar wind and at the Earth's flank magnetopause when shear flow and density asymmetries are present.

[21] A finite shear flow that results in a stronger J_M of the bounding current sheet pair on the low-density side of reconnection exhausts (see Figures 2 and 4) also explains the magnitude of the B_L magnetic field component within oppositely directed exhausts at Wind and ST-A on 11 March 2007.

[22] **Acknowledgments.** We thank R. P. Lepping, R. P. Lin, and K. W. Ogilvie for the use of Wind data made available via CDAWeb and the reviewers for their constructive suggestions. This work is supported by NASA grant NNX07AH72G at the University of Colorado at Boulder.

[23] Zuyin Pu thanks Antonius Otto and another reviewer for their assistance in evaluating this paper.

References

Acuña, M. H., D. Curtis, J. L. Scheifele, C. T. Russell, P. Schroeder, A. Szabo, and J. G. Luhmann (2008), The STEREO/IMPACT magnetic field experiment, *Space Sci. Rev.*, *136*, 203, doi:10.1007/s11214-007-9259-2.

Galvin, A. B., et al. (2008), The plasma and suprathermal ion composition (PLASTIC) investigation on the STEREO observatories, *Space Sci. Rev.*, *136*, 437, doi:10.1007/s11214-007-9296-x.

Gosling, J. T., and A. Szabo (2008), Bifurcated current sheets produced by magnetic reconnection in the solar wind, *J. Geophys. Res.*, *113*, A10103, doi:10.1029/2008JA013473.

Gosling, J. T., R. M. Skoug, D. J. McComas, and C. W. Smith (2005), Direct evidence for magnetic reconnection in the solar wind near 1 AU, *J. Geophys. Res.*, *110*, A01107, doi:10.1029/2004JA010809.

Gosling, J. T., et al. (2006a), Petschek-type reconnection exhausts in the solar wind well beyond 1 AU: Ulysses, *Astrophys. J.*, *644*, 613.

Gosling, J. T., S. Eriksson, and R. Schwenn (2006b), Petschek-type magnetic reconnection exhausts in the solar wind well inside 1 AU: Helios, *J. Geophys. Res.*, *111*, A10102, doi:10.1029/2006JA011863.

Gosling, J. T., S. Eriksson, T. D. Phan, D. E. Larson, R. M. Skoug, and D. J. McComas (2007a), Direct evidence for prolonged magnetic reconnection at a continuous X-line within the heliospheric current sheet, *Geophys. Res. Lett.*, *34*, L06102, doi:10.1029/2006GL029033.

Gosling, J. T., S. Eriksson, L. M. Blush, T. D. Phan, J. G. Luhmann, D. J. McComas, R. M. Skoug, M. H. Acuna, C. T. Russell, and K. D. Simunac (2007b), Five spacecraft observations of oppositely directed exhaust jets from a magnetic reconnection X-line extending >4.26 10^6 km in the solar wind at 1 AU, *Geophys. Res. Lett.*, *34*, L20108, doi:10.1029/2007GL031492.

Karimabadi, H., D. Krauss-Varban, N. Omidi, and H. X. Vu (1999), Magnetic structure of the reconnection layer and core field generation in plasmoids, *J. Geophys. Res.*, *104*, 12,313.

Knetter, T., F. M. Neubauer, T. Horbury, and A. Balogh (2004), Four-point discontinuity observations using Cluster magnetic field data: A statistical survey, *J. Geophys. Res.*, *109*, A06102, doi:10.1029/2003JA010099.

La Belle-Hamer, A. L., A. Otto, and L. C. Lee (1995), Magnetic reconnection in the presence of sheared flow and density asymmetry: Applications to the Earth's magnetopause, *J. Geophys. Res.*, *100*, 11,875.

Lepping, R. P., et al. (1995), The Wind magnetic field investigation, *Space Sci. Rev.*, *71*, 207.

Levy, R. H., H. E. Petschek, and G. L. Siscoe (1964), Aerodynamic aspects of the magnetospheric flow, *AIAA J.*, *2*, 2065.

Lin, C. C., H. Q. Feng, D. J. Wu, J. K. Chao, L. C. Lee, and L. H. Lyu (2009), Two-spacecraft observations of an interplanetary slow shock, *J. Geophys. Res.*, *114*, A03105, doi:10.1029/2008JA013154.

Lin, R. P., et al. (1995), A three-dimensional (3-D) plasma and energetic particle experiment for the Wind spacecraft of the ISTP/GGS mission, *Space Sci. Rev.*, *71*, 125.

Lin, Y., and L. C. Lee (1994), Structure of reconnection layers in the magnetosphere, *Space Sci. Rev.*, *65*, 59.

Ogilvie, K. W., et al. (1995), SWE, a comprehensive plasma instrument for the Wind spacecraft, *Space Sci. Rev.*, *71*, 41.

Paschmann, G., et al. (1979), Plasma acceleration at the Earth's magnetopause: Evidence for magnetic reconnection, *Nature*, *282*, 243.

Paschmann, G., I. Papamastorakis, W. Baumjohann, N. Sckopke, C. W. Carlson, B. U. Ö. Sonnerup, and H. Lühr (1986), The magnetopause for large magnetic shear: AMPTE/IRM observations, *J. Geophys. Res.*, *91*, 11,099.

Phan, T. D., et al. (2006), A magnetic reconnection X-line extending more than 390 Earth radii in the solar wind, *Nature*, *439*, 175.

Priest, E., and T. Forbes (2000), *Magnetic Reconnection: MHD Theory and Applications*, Cambridge Univ. Press, New York.

Sonnerup, B. U. Ö., and M. Scheible (1998), Minimum and maximum variance analysis, in *Analysis Methods for Multi-Spacecraft Data*, edited by G. Paschmann and P. W. Daly, *ISSI Sci. Rep. SR-001*, pp. 185–220, Eur. Space Agency Publ. Div., Noordwijk, Netherlands.

Sonnerup, B. U. Ö., G. Paschmann, I. Papamastorakis, N. Sckopke, G. Haerendel, S. J. Bame, J. R. Asbridge, J. T. Gosling, and C. T. Russell (1981), Evidence for magnetic field reconnection at the Earth's magnetopause, *J. Geophys. Res.*, *86*, 10,049.

L. M. Blush, Space Research and Planetary Sciences Division, Physikalisches Institut, University of Bern, Sidlerstrasse 5, CH-3012, Bern, Switzerland.

S. Eriksson and J. T. Gosling, Laboratory for Atmospheric and Space Physics, University of Colorado at Boulder, 1234 Innovation Drive, Boulder, CO 80303-7814, USA. (eriksson@lasp.colorado.edu)

A. B. Galvin and K. D. C. Simunac, Space Science Center, University of New Hampshire, Morse Hall, 39 College Road, Durham, NH 03824-3525, USA.

D. Krauss-Varban, J. G. Luhmann, and T. D. Phan, Space Sciences Laboratory, University of California, 7 Gauss Way, Berkeley, CA 94720-7450, USA.

C. T. Russell, Institute of Geophysics and Planetary Physics, University of California, 405 Hilgard Avenue, Los Angeles, CA 90095, USA.

A. Szabo, Heliospheric Physics Laboratory, NASA Goddard Space Flight Center, Code 672, Greenbelt, MD 20771, USA.